Integration of Lunar Polar Datasets

Stewart Nozette: Naval Research Laboratory, Washington D.C.
Chris Lichtenberg: Naval Research Laboratory, Washington D.C.
Paul D. Spudis: Lunar and Planetary Institute, Houston TX
Mark S. Robinson: Northwestern University, Evanston IL
D.B.J. Bussey: Northwestern University, Evanston IL; ESTEC European Space Agency, Noordwijk, The Netherlands
Robert Bonner: Protasis Inc, Alexandria VA

Abstract

Newly processed Clementine bistatic radar data are co-registered with lunar polar illumination data, Arecibo ground-based monostatic radar data, and Lunar Prospector neutron spectrometer measurements. We find that Epithermal neutron flux anomalies are coincident with permanently shadowed regions at the lunar south pole and these areas also correlate with the β=0 Circular Polarization Ratio (CPR) enhancements revealed by processing of Clementine bistatic radar echoes obtained during lunar orbit 234, which in turn are co-located with areas of anomalous high CPR observed by Arecibo Observatory on the lower, sun-shadowed wall of Shackleton crater. Additionally, Shackleton crater is located within a region identified as having an enhanced hydrogen content by the Lunar Prospector Neutron Spectrometer. Estimates of the extent of high CPR from Arecibo Observatory and Clementine radar data independently suggest approximately 10 km^2 of ice may be present on the inner Earth facing wall of Shackleton crater. None of the experiments that obtained the data presented here were ideally suited for definitively identifying ice in lunar polar regions. However, by assessing the relative merits of all available data we find that it is plausible that ice does occur in cold traps at the lunar south pole, and that future missions with instruments specifically designed to investigate these anomalies is worthy.

Introduction

The lunar poles have long been theorized to harbor ice deposits in permanently shadowed regions [*Watson et al.*, 1961]. This is a fascinating possibility, as such deposits would serve as a rich natural resource for future lunar colonists. Unfortunately the poles of the Moon are extremely difficult to observe from the Earth, and no lunar orbiting spacecraft experiments have been specifically designed to unambiguously detect ice in the lunar polar regions. However, several experiments have returned data pointing to anomalies in these regions, but these results are controversial. Initially, Arecibo monostatic circular polarization ratio (CPR) radar observations in the region of the lunar south pole were interpreted to possibly indicate the presence of ice deposits on the lower Earth facing interior wall of Shackleton crater[28]. Data collected by the Clementine Bistatic radar experiment[14,20] also revealed anomalous polarization ratios in the Shackleton region, suggesting the presence of patchy, "dirty", ice deposits. Subsequently, the same Arecibo data utilized in Stacy [1993] were reported to be inconsistent with this interpretation[29]. There it was suggested that all anomalous high CPR areas observed by Arecibo, near the lunar south pole, were caused by rough surfaces as only some portions of the anomalies were believed to be permanently shadowed. Additionally, *Simpson and Tyler* [1999] postulated that the Clementine polarization anomaly was due to roughness and/or random noise in the data and not by the presence of ice.

The Arecibo monostatic CPR data suggest areas of CPR enhancement associated with slopes inclined towards Earth, such as the radar facing walls of impact craters, and prominently seen in Shackleton crater (89.6°S, 110.0°E). The high CPR region deepest within Shackleton has a local radar angle of incidence of ~50° and a monostatic CPR of 1.19 +/- 0.12 [28], comparable to the high CPR feature at the north pole of Mercury measured by *Harmon and Slade* [1992]. *Stacy* [1993] noted that since this area may be permanently shadowed, Coherent Backscatter Opposition Effect (CBOE) from ice deposits may be responsible for the enhanced CPR echo within Shackleton crater. The Arecibo CPR images also show many small areas with high CPR ratios between 0.9 and 1.0, associated with the radar bright ejecta of small impact craters, that are *not* in permanent shadow. For this reason *Stacy et al.* [1997] suggested wavelength scale surface roughness as an alternative to ice as a scattering mechanism. However, if the enhanced backscatter in Shackleton crater has a contribution from ice there should be differences in scattering properties between areas in sunlight and areas in permanent shadow. *Stacy* [1993] does report a statistically significant increase in monostatic Right Circular Polarization (RCP) radar cross-section (2.4 dB) and CPR (10%) in the scattering

measured on the lower solar shadowed interior wall (relative to the illuminated upper rim) in Shackleton crater. This same increase in RCP cross section while traversing from the solar illuminated rim down into solar shadowed wall was found in other craters near the poles[28]. This is opposite of that observed in impact craters where the entire interior crater wall is illuminated (e.g. craters in Sinus Iridium, 45°N 40°W). In these craters the upper part of the radar facing inner rims of solar illuminated craters have 1-3 dB greater backscatter cross-sections than the lower portions of the same crater walls[28]. From these observations *Stacy* [1993] concluded that either the south polar craters, including Shackleton, have an unusual morphology, or that radar backscatter is enhanced by ice located further down from the crater rim in regions of permanent shadow. It is important to remember that the anomalies identified by *Stacy* [1993] were small relative to the radar resolution cell, usually a few to a dozen contiguous pixels.

Recent theoretical analysis[5] supports the idea of extant ice deposits on the Moon and Mercury in permanently shadowed regions. The use of bistatic measurements to differentiate high CPR caused by CBOE from high CPR resulting simply from wavelength scale surface roughness is well documented[12]. Deposits of meter scale low loss material (e.g. ice) produce CBOE. The Lunar Prospector neutron spectrometer experiment measured epithermal neutron flux consistent with significant (1850 km^2, 2m thick) dirty ice deposits in shadowed areas at both lunar poles[9]. Fast neutron deficits associated with the south pole region indicate such deposits could be within 10 cm of the surface. Alternatively, a solar wind enhancement mechanism might account for the epithermal neutron anomalies observed by Lunar Prospector. However, solar wind enhancements would not produce CBOE as the solar wind hydrogen enriched regolith would not be low loss at radar wavelengths. Additionally, there is no known mechanism to preferentially collect solar implanted H in permanently shadowed regions. Groundbased monostatic radar[28], Clementine bistatic radar data[20, 21], and Lunar Prospector neutron spectrometer data[9, 10] all have been interpreted as suggesting that patchy ice covered and/or mixed with regolith is present at the lunar south pole.

To shed light on the question - "does ice exist in permanently shadowed craters" – we coregistered image and shadow maps with neutron spectrometer, groundbased, and Clementine bistatic radar data to investigate possible correlations and apparent contradictions, and differing interpretations by various workers (outlined above)[20,24,28,29]. Less accurate control networks hampered previous analyses [e.g. [29]], thus we use an improved control network[3,4] to compare data. Accurate geographic control is key to understanding the degree to which monostatic and bistatic CPR enhancements are correlated with shadows or other surface features. Additionally, new processing of the Clementine Bistatic radar data has improved the spatial resolution through selective binning of individual Bistatic targets which lie on the ß=0 track. Final high-resolution Lunar Prospector data have improved spatial resolution such that neutron anomalies can now be correlated with surface features near the poles[10].

Description of Datasets

Control Network

Previous correlation of radar features and shadowed terrain were not optimal due to the preliminary control networks then available. For example, Arecibo radar images of the poles were tied to the Lunar Orbiter control network[29], resulting in poor correlation when comparing features observed in Clementine and Arecibo radar data, resulting in mis-location of more than 10 km^3. Also, during construction of illumination maps it was determined that the previous USGS-RAND global Clementine control network[8] was not optimal within a few degrees of the poles[3,4]. In order to locally improve the network, Arecibo radar images (one each at the north and south poles[29]) that represented the maximum surface coverage of the polar regions (from 80° to the pole on the nearside, with lesser coverage on the farside) available in single images were used. They were controlled to the USGS basemap[8] in the vicinity of 80-85° where the global control network is more reliable. Near the poles (85°-90°) the Clementine images were then tied to the newly controlled radar images[3,4]. Subsequent improvements in the polar control network and the addition of HIRES image data allow improved limits to be placed on the location and distribution of permanently shadowed terrain[3,4].

Lunar Prospector Neutron Spectrometer Dataset

Lunar Prospector neutron spectrometer datasets were obtained at low altitude (30 km) during the extended mission[10]. These include both epithermal and fast neutron flux measurements. These are plotted as color-coded maps that depict the epithermal neutron counts arising from latitude/longitude cells projected on the lunar polar regions. These low altitude data have a factor of 3 better resolution thus greatly increasing the capability of co-registering neutron deficits with surface features such as permanently shadowed craters.

Solar Illumination Dataset

Bussey et al. [1999a,b] created an illumination map was created by co-adding all the images near the pole that had common overlap and then looking for areas which receive no illumination, enabling better isolation of areas likely to be in permanent shadow. Their best current estimate of the maximum extent of shadow at the south pole is 3300 km^2 within 1.5 ° of the pole. The corresponding number for the north pole is 530 km^2 [20] which is an initial estimate based on the area of a few craters close to the pole that appear to be permanently shadowed. Subsequent work has shown that features such as small crater floors, and north facing crater rims might be in permanent shadow[4]. This appears true for features all the way out to 80°N. A preliminary darkness map shows that there are numerous small outcrops of shadow with a total area of approximately 10,000 km^2 within 10° of the pole[4].

Clementine Bistatic Radar Dataset

The Clementine bistatic radar experiment and data processing methodology is described in detail in *Lichtenberg* [2000]. This experiment measured the radar scattering properties of the lunar surface as a function of bistatic angle, ß. Initial analysis of the bistatic radar data[20] used averages over broad areas of polar terrain. New processing has improved the spatial resolution and allows rough geographic correlation of anomalies with specific terrain features. Figure 1 shows the locus of points sampled by Clementine during orbits 234 and 235. These data are overlaid on top of an Earth based radar image in order to provide geographical context. The Clementine Bistatic radar data was dynamically processed to extract an average CPR vs. ß for specific surface areas[14]. The areas which contain the ß=0 track were sampled at a range of ß angle. To detect CBOE, terrain must be sampled around ß ± 1-2°. Only CBOE originating from terrain visible by the Earth receiving stations, lying along the Clementine ß=0 ground track, will be detectable in the Clementine bistatic radar dataset. Rainbow colored areas (Figures 1,2, A1) show the regions sampled where ß has a value between +1° and – 1°, with terrain sampled at minimum beta lying under the ß=0 track, for orbit 234 and orbit 235. The most reliable CBOE measurements come from the center of these regions. The colored horseshoe shaped areas represents the territory over which the average sample was taken over time. Orbit 235 does not sample any areally significant polar shadowed terrain and thus serves as a control orbit.

Figures 2a and 2b show some of the bistatic radar results in more detail (the remaining sample sites are presented in the Appendix for completeness). These data indicate the nature of the radar return for several of the sampling stations for both orbit 234 and orbit 235. Target 17 in orbit 234 covers the Earth facing inner wall of Shackleton crater. Figure 2b shows that target 17 has the highest enhancement of CPR at ß=0 of any of the Clementine targets. Target 16 in orbit 234, which covers a large fraction of the floor of Shackleton crater, as well as the inner wall that faces away from Earth (and therefore can't be observed by Earth based radar ground stations) also has a detectable CPR as ß approaches zero.

Arecibo Monostatic Radar Dataset

The Arecibo monostatic RCP, LCP and CPR images for south poles were first published in *Stacy* [1993]. These data give a much better picture of the geography around the pole than can be seen in the Clementine images due to the large amount of solar shadowing. The shadowing at the south pole was at a maximum during the Clementine mission as it was southern winter. Despite the poor viewing geometry of the lunar poles from Earth, the radar data can see into solar shadowed regions in many areas (Figure 3). Near the pole the radar advantage diminishes and only a sliver of the solar shadowed area on the inner Earth facing wall in Shackleton can be seen in the radar images[28]. Of special interest are the areas of overlap between solar shadowed terrain and areas visible to Earth based radar receivers. Such area(s) are the only possible sources of ice signals (if ice exists at the poles) in the radar datasets. The CPR image was thresholded to isolate CPR regions in the range 0.9-1.1 (Figure 3LR) identified by *Stacy* [1993] as potentially emanating from ice bearing materials. The largest concentration of the CPR anomalies are related to the Earth facing inner wall of Shackelton. Examination of solar shadow data and the CPR map show that ~46 km^2 of solar shadowed terrain within Shackleton crater can be observed. This estimate is in agreement with independent estimates derived from ground based radar interferometry topography.

Discussion

By combining the radar, illumination, and neutron spectrometer datasets we can constrain the distribution and physical state of putative ice deposits. The coregistered datasets are presented in Figures 3-5. Figure 4 consists of a south pole composite image of shadowed areas, the orbit 234 ß=0 ground-track, and the Arecibo CPR ≈ 1 areas. Figure 5 shows the Lunar Prospector neutron spectrometer flux measurements from Feldman et al. [1999] with the location of

Shackleton and neighboring craters also shown. The neutron data (Figure 5) show a general regional epithermal neutron deficit correlated with areas of permanent shadow at the poles[9,10]. The Lunar Prospector neutron spectrometer data reveal three distinct anomalies associated with Shackleton crater and two adjacent craters. One of the three anomalous NS sample elements at the south pole covers a major portion of Shackleton crater (Figure 5). Approximately 1km^2 of relatively pure ice (10-20% regolith), with a shallow regolith covering (10-20 cm), should be detectable by the Clementine bistatic radar experiment[24]. Therefore, a few percent of the Lunar Prospector estimated ice area should be detectable by Clementine Bistatic radar, given favorable location and geometry

The areas of high CPR (~1) observed by Arecibo occur in both shadowed and illuminated areas as previously noted[29]. However, these areas are not all identical in morphology and geological context. Arrows in Figure 4 show the largest areas of contiguous high CPR on the lower wall of Shackleton crater. The correlation of the largest contiguous observed area of high CPR and the close coincidence of the Clementine orbit 234 ß=0 track is also shown in Figure 4. The largest area of contiguous high CPR is associated with the shadowed lower wall of Shackleton crater, which we estimate to be 10± 6 km^2, based on a range of pixel counts and thresholds from the region. The ~ 1dB, ß=± 1□, bistatic CPR enhancement in target 17 (Figure 2b) is the most CBOE like found in the Clementine Bistatic radar data set. It also samples the same location (Figure 4), which contains the anomalous high CPR areas reported in the lower Earth facing rim of Shackleton[28]. Of the Clementine bistatic analysis targets, target 17 has the closest, non-overlapping proximity to the Earth facing wall of Shackleton crater. The area sampled by target 17, ß± 1°, is calculated to be 5130 km^2. This is the average of the sampled area for which ß is ±1° and for which a Doppler frequency bin coincides with that of target 17.

Target 17 is the target that best covers the Earth facing inner wall of Shackleton, specifically including the areas of Arecibo high CPR. Figure 2b shows that target 17 has a high Clementine CPR enhancement approaching ß=0. Additionally target 16 (Figure 2b) also shows a noticeable Clementine CPR enhancement approaching ß=0. It covers a large portion of the floor of Shackleton as well as the crater wall that faces away from Earth (not visible from Earth based radar receivers), both regions that are permanently shadowed and therefore possible locations of ice deposits. A series of targets (1-10) obtained during Clementine orbit 235 sample virtually no polar shadowed terrain which is otherwise similar to the orbit 234 ground track terrain, both are cratered highlands (Figure 2a). Orbit 235 serves as a control area. These areas show no statistically significant (3Ó 0.3dB) ß± 1° CPR enhancements.

The method applied to estimating the fractional ice area on Mercury[6] was applied to target 17 (orbit 234, Figure 2b). Using the specific radar cross sections of average illuminated lunar surface measured during Clementine control orbit 235 for a region of latitude –80° to -82° and ß± 1°, radar properties attributed to ice on Mercury, and the relative CPR enhancement in orbit 234 target 17 (1±0.3dB), a fractional area for the observed ice surface area is estimated. The fractional ice area which could produce the observed target 17 ß± 1° CPR enhancement is ≈10-16 km^2. This estimate is in agreement with the area of anomalous high CPR area observed in Shackleton crater by Arecibo (10± 6 km$^{2)}$, and is an order of magnitude greater than the minimum Clementine detection threshold. It is likely the high CPR regions in Shackleton contribute to the average CPR enhancement reported by *Nozette et al.* [1996], and the sporadic CPR enhancements reported subsequently[24]. The Clementine bistatic CPR enhancement is largely due to enhanced RCP (Figure 2, Appendix), suggesting the high radar backscatter is due to CBOE[16]. RCP is more indicative of surface composition for measurements at large incidence angles[16].

It has been argued on theoretical[1,5,13] and observational[6] grounds that "dirty" ice deposits are present in the permanently shadowed regions near the north pole of Mercury. It was suggested[11] that if ice deposits of the magnitude postulated for Mercury are present on the moon they should be detectable by Earth-based radar. *Feldman et al.* [1998] argues that lunar polar radar ice measurements are indeterminate due to a covering high FeO regolith (not found on Mercury). No direct compositional data exist for Mercury, however remote sensing measures indicate that the mercurian crust is most likely similar to lunar highlands material (low FeO anorthositic material; e.g. [30,27]). Finally, FeO regolith content has been shown to have little effect on 13 cm radar observations probing similar depth as the neutron spectrometer measurements[7].

One possible explanation for the differences in lunar and mercurian radar observations is the observing geometry. The relatively high angle of incidence of existing lunar radar measurements (~ 85° for Arecibo and Clementine, vs. ~70-80° for Mercury,) limits the

observable shadowed area, making Earth-based lunar observations much less distinctive than on Mercury. High radar incidence angles (~85°) and slightly higher regolith mixing fraction will suppress the lunar polar CBOE effect (Figure 6). Theory suggests the most likely permanently shadowed lunar areas must be closest to the pole[1, 25]. The actual areas of permanent shadow and radar observable ice deposits are the results of topography that limit Earth based observations. The unique Clementine bistatic geometry and the fortuitous sampling of the most anomalous high CPR area within a topographically controlled, Earth facing, polar shadowed area having a reduced angle of incidence (50°), allowed the detection of a weak CBOE (and ice) at the south pole by Clementine; a detection consistent with the Lunar Prospector neutron spectrometer data.

Summary and Conclusions

The co-registration of lunar south pole remote sensing datasets shows the interior wall of Shackleton crater to be unique. Refined processing of the Clementine bistatic radar data into higher resolution geographic bins shows the highest bistatic CPR enhancement around ß=0 originates in this anomalous region in the lower Earth facing wall Shackleton crater. The geographic coincidence of the Clementine bistatic ß=0 track directly with the Arecibo high CPR anomaly discovered by *Stacy* [1993] is coincident with the enhanced CPR observed by the Clementine bistatic radar experiment for orbit 234. Areal estimates of high CPR from pixel counts of Arecibo data, and independent estimates based on the Clementine radar results, using the fractional area of high CPR (0.9-1.1) required to yield the observed 1dB CPR enhancement for the area sampled in Clementine target 17, are consistent. The bistatic dependence of CPR and RCP supports the conclusion that the high CPR observed in the monostatic and bistatic radar data sets, containing the lower Earth facing wall of Shackleton, is suggestive of CBOE and therefore of "dirty" ice rather than wavelength (cm) scale roughness. When the high resolution Lunar Prospector Neutron Spectrometer data[10] are integrated with the radar and sun shadow data sets, the results show that Shackleton crater is contained within the anomalous epithermal and fast neutron deficit region adjacent to the lunar south pole.

While the dataset integration provides supporting evidence for the presence of ice on the lower wall of Shackleton[28,20], it is not conclusive. Corroboration of this hypothesis requires additional data. Earth-based radar experiments (as well as orbiters that use an Earth receiver, i.e. Clementine) are limited in that the surface visible from Earth represents only a small portion of the permanently shadowed terrain, e.,g less than 10% in the case of Shackleton. The grazing incidence angle means that CBOE is muted (Figure 6) and back and forward scattering mechanisms are likely dominated by surface structure (e.g. cm scale roughness) rather than composition. The optimum incidence angle to detect CBOE would be near 45° where neither the quasi-specular or diffuse backscatter components dominate the echo. This could be accomplished by an orbiting synthetic aperature radar which measures CPR and RCP and LCP for a range of incidence angles around 45°, with a resolution of 100m or better. Such an experiment could distinguish ice from dry lunar surface by optimal viewing of the entire permanently shadowed region. Such future observations when combined with higher resolution neutron spectrometer data will allow optimum targeting of in-situ measuements. These will conclusively determine the composition, origin, and areal distribution of the anomalies (ice?) identified at the lunar poles, allowing for the next steps of exploration and utilization by humans. The significance of the Shackleton region for future human exploration and utilization can be seen in Figure 7. The illumination map (Bussey et al 1999) and the putative anomlous areas on the lower wall of Shackleton are shown in the composite image. The three areas (A,B,C) of near constant illumination are within 10 km of the putative ice deposits on the lower Earth facing wall of Shackleton It can be seen that one of these three areas is always illuminated during the lunar day. The periods of shadow are much shorter than the equatorial lunar night and the low sun produces a relativly benign thermal environment. Permanentl long shadows also will allow for safer landings. Energy storage for the maximum period of shadow at any of the regions is much less than 14 days. Additionally, a power grid could connect points A,B,C to provide constant energy to a base on the rim of Shackleton. The juxtaposition of a near constant solar energy source and the presence of ice suggest this area may be the most habitable region for the first human extraterrestrial outpost.

Acknowledgements: This manuscript benefited from useful discussions with W. Feldman, A. Binder, D.B. Campbell, N.J.S. Stacy, R.A. Simpson, G.H. Pettengill, I.I. Shapiro, R. Jurgens, and M. Slade. We thank N.J.S. Stacy for providing the Arecibo radar data. The Advanced Systems Office, NASA Johnson Space Center, under contract T-250W, supported this work. Additional support was furnished by the Naval

Research Laboratory. This paper is Lunar and Planetary Institute Contribution 99 - 1059.

---

[1] Arnold, J.R., Ice in the lunar polar regions, *J. Geophys. Res.*, 84, 5659-5668, 1979.

[2] Binder, A. B. Lunar Prospector: Overview, *Science* 281: 1475-77,1998.

[3] Bussey D.B.J., P.D. Spudis , and M.S. Robinson, Illumination conditions at the lunar south pole, *Geophys. Res. Letters* , 26,1187-1190, 1999a.

[4] Bussey D.B.J., M.S. Robinson, P.D. Spudis, Illumination conditions at the lunar poles, *Lunar and Planetary Sci XXX*, (CD-ROM) abstract 1731, 1999b.

[5] Butler B, The migration of volatiles on the surfaces of Mercury and the Moon, *J. Geophys. Res.*, 102, 19283-19291, 1997.

[6] Butler B., D.O. Muhleman, and M.Slade, Mercury: Full disc radar images and the detection and stability of ice at the north pole, *J. Geophys Res.*, 98, 15,003-15,023, 1993.

[7] B.A. Campbell, B.R. Hawke, T.W. Thompson, Regolith composition and structure in the lunar maria: Results of long-wavelength radar studies, *J. Geophys. Res.*, 102, 19307-19320, 1997.

[8] Edwards, K.E., T.R. Colvin, T.L. Becker, D. Cook, M.E. Davies, T.C. Duxbury, E.M. Eliason, E.M. Lee, A.S. McEwen, H. Morgan, M.S. Robinson, T. Sorensen, Global digital mapping of the Moon (abstract), in *Lunar and Planetary Science XXVII*, Lunar and Planetary Institute, Houston, 1996.

[9] Feldman, W. C., S. Maurice, A.B. Binder, B.L. Barraclough, R.C. Elphic, D.J. Lawrence, Fluxes of Fast and Epithermal Neutrons from Lunar Prospector: Evidence for Water Ice at the Lunar Poles, *Science*, 281: 1496-1500, 1998.

[10] Feldman, W.C., S. Maurice, D.J. Lawrence, I. Getenay, R.C. Elphic, B.L. Barraclough, A.B. Binder, Enhanced Hydrogen Abundances Near Both Lunar Poles (abstract), *in New Views of the Moon II: Understanding the Moon through the integration of diverse datasets*, September 22-24, 1999, Flagstaff AZ, Lunar Planetary Institute, Houston, CD-Rom abstract 8051, 1999.

[11] Harmon, J.K., Mercury radar studies and lunar comparisons, *Adv. Space Res.*, 19, 10, 1487-1496, 1997.

[12] Hapke, B. and D. Blewett, Coherent backscatter model for the unusual radar reflectivity of icy satellites, *Nature*, 352, 46-47, 1991

[13] Ingersoll, A.P., T. Svitek, and B.C. Murray, Stability of polar frosts in spherical bowl-shaped craters on the Moon, Mercury, and Mars, *Icarus*, 100, 40-47, 1992.

[14] Lichtenberg C.L. *Bistatic Radar Observations of the Moon Using the Clementine Spacecraft and Deep Space Network* , Ph.D thesis, Johns Hopkins Univ. 2000.

[15] Mishchenko, M. I., Physically based computations of coherent backscatter, *J. Quant.Spectrosc.Radiat. Transfer* , 57,767-57,777, 1996.

[16] Mishchenko, M. I., Personal Communication, 1997.

[17] Mishchenko, M. I., Polarization characteristics of the coherent backscatter opposition effect, *Earth, Moon, and Planets*, *58*, 127-144, 1992a.

[18] Mishchenko, M. I., The angular width of the coherent back-scatter opposition effect: an application to icy outer planet satellites, *Astrophysics and Space Science*, *194*, 327-333, 1992b.

[19] Mishchenko, M. I., Diffuse and coherent backscattering by discrete random media-I. Radar reflectivity, polarization ratios, and enhancement factors for a half-space of polydisperse, nonabsorbing and absorbing spherical particles, *Journal of Quantitative Spectroscopy and Radiative Transfer*, *56*, 673-702, 1996.

[20] Nozette S., C.L. Lichtenberg, P.Spudis, R. Bonner, W. Ort, E. Maleret, M. Robinson, and E.M.Shoemaker, The Clementine Bistatic radar experiment, *Science*, 274, 1495-1498, 1996.

[21] Nozette S., E. M. Shoemaker, P. Spudis, C.L. Lichtenberg, The possibility of ice on the moon, *Science*, 278, 144-145, 1997.

[22] Nozette, S., C.L. Lichtenberg, R. Bonner, P. Spudis, and M. Robinson, Comments on radar search for ice at the lunar south pole by R. Simpson and G.L. Tyler, in *Integrated remote sensed geophysical and sample*

datasets, Lunar and Planetary Institute, LPI Contribution 958, 1998.

[23] Peters, K. J., The coherent backscatter effect: a vector formulation accounting for polarization and absorption effects and small or large scatterers, *Physical Review B, 46*, 801-809, 1992.

[24] Simpson R.A. and G.L. Tyler , 1999., Reanalysis of Clementine Bistatic radar data for the lunar south pole, *J. Geophys Res.,* 104, 3845-3862, 1999.

[25] Smith, D.E., M.T. Zuber, G.A. Neumann, and F.G. Lemoine, Topography of the Moon from Clementine lidar, *J. Geophys. Res.*, 102, 1591-1611, 1997.

[26] Shoemaker E.M., M.S. Robinson, E.M. Eliason, The south pole region of the moon as seen by Clementine, *Science* , 266, 1851-54, 1994.

[27] Sprague, A.L., R.W.H. Kozlowski, F.C. Witteborn, D.P. Cruikshank, D.H. Wooden, Mercury, Evidence for anorthosite and basalt from mid-infrared (7.3-13,5) spectroscopy, *Icarus*, 109, 156-197, 1994.

[28] Stacy, N.J.S., *High-resolution synthetic aperture radar observations of the moon*, PhD thesis , Cornell Univ. 1993.

[29] Stacy, N. J. S., D.B. Campbell, P.G. Ford, Arecibo Radar Mapping of the Lunar Poles: A Search for Ice Deposits, *Science*, 276, 1527-1530, 1997.

[30] Vilas, F., Surface composition of Mercury from reflectance spectrophotometry, in *Mercury* (F. Vilas, C. Chapman, M.S. Mathews, eds), Univ. Arizona Press, 1988.

Figure Captions

Figure 1. Overall view of the lunar south pole showing locations of Clementine radar sampling targets for orbits 234 and 235 overlain on Arecibo radar reflectivity image [*Stacey*, 1993]. The frequency spectra were collected during analysis into 4-second wide bins within which each frequency bin was 3.05 Hz wide. The width of the colored regions along the beta zero track depicts the overlap of all bins containing the targets during the almost 200 seconds that each was within $\pm 1°$ of ß=0°. The breadth of the colored regions across track is the limit of the $\pm$ 1° constraint, blue to red represents 1° to 0°, respectively. The yellow lines indicate the □=0 track for each orbit and the red circle shows the approximate size of the Lunar Prospector 2 degree data [Feldman et al., 1999; 2000]. S indicates the location of Shackleton crater, U1 and U2 refer to craters called out in Feldman et al. [2000] as possible sources of neutron spectrometer anomalies.

Figure 2a. Clementine bistatic radar response plots and sampled regions for targets 1-4 from orbit 235 overlain on the Arecibo OS radar image shown in detail (see overall location and explanation in **Figure 1**). Orbit 235 radar sampling regions contain little to no resolved permanently shadowed regions and thus serves as control for data from orbit 234. **2b.** Clementine bistatic radar targets 14-17 orbit 234, note the gradually increasing and sharpening of the signal as the ß=0 track passes over Shackleton crater, same region where Arecibo RCP data first showed the crater wall to be anomalous [*Stacey*, 1993]. On the response plots solid line represents CPR, upper dashed line is LCP, while lower dashed line is RCP (for all plots in a and b). The rest of the orbit 234 and 235 samples are presented in the Appendix.

Figure 3. (UL) Arecibo radar reflectance image [*Stacey*, 1993] of the lunar south pole region. S indicates the location of Shackleton crater, U1 and U2 refer to craters called out in *Feldman et al.* [2000] as possible sources of neutron spectrometer anomalies. **(UR)** Same radar image as in UL with RCP/LCP ratio anomalies identified from image published in *Stacy* [1993]. **(LL)** UVVIS summation map indication relative amount of sunlight per pixel during one lunar day, brighter pixels indicate greater illumination and black represents shadowed regions (during lunar winter) [*Bussey et al.*, 1999a]. **(LR)** Composite overlay of radar brightness (background), UVVIS summation light map, Arecibo RCP/LCP anomaly (red-orange dots) with a more conservative threshold (~0.9 to 1.0) than shown in UR, Clementine orbit 234 bistatic radar □=0 track (blue line). And Earth-based radar shadow regions derived from same UL (stipple pattern).

Figure 4. Close-up of south pole region showing the anomalous Arecibo high CPR areas (orange to red dots) in and near Shackleton crater (arrow), the radar shadowed region (tan) and the Clementine orbit 234 bistatic radar ß=0 track (blue line), overlain on the UVVIS summation light map. White circle is 85°S latitude.

Figure 5. (L) Lighting map overlaid on Clementine UVVIS mosaic, blue line indicates the Clementine orbit 234 ß=0 track, crater labels same as **Figure 1**. **(R)** Epithermal neutron flux measurements from Lunar Prospector. The blue areas represent flux deficits reflecting higher concentrations of H. South polar craters which contain permanently shadowed terrain are labeled along with Shackleton "S" [adapted from http://www.lunar.lanl.gov/, see also *Feldman et al.* [1999].

Figure 6. Peak Broadening of CBOE resulting from the non-ideal incidence angles when observing both the poles of the Moon (85°) and Mercury (79°) from the Earth [adapted from *Lichtenberg*, 2000; see also *Peters* 1992, *Mischenko* 1992a,b, 1996]. Note that while still poor, the viewing angle and thus CBOE peak is more well defined for the mercurian rather than the lunar case and that the mercurian observing angles actually range from ~70° to 80°.

Figure 7. Composite image of the region surrounding Shackleton. The illumination map (left) taken from Bussey et al (1999a,b) showing illuminated (yellow) and shadowed (black) intervals (10 hr) over the course of a lunar day. Regions A,BC, are shown by arrows. The anomolous CPR areas are shown in orange on the lower Earth facing wall of Shackleton. The juxtaposition of near constant illuminated areas with the putative ice deposits suggests this region is well suited to an initial lunar base.

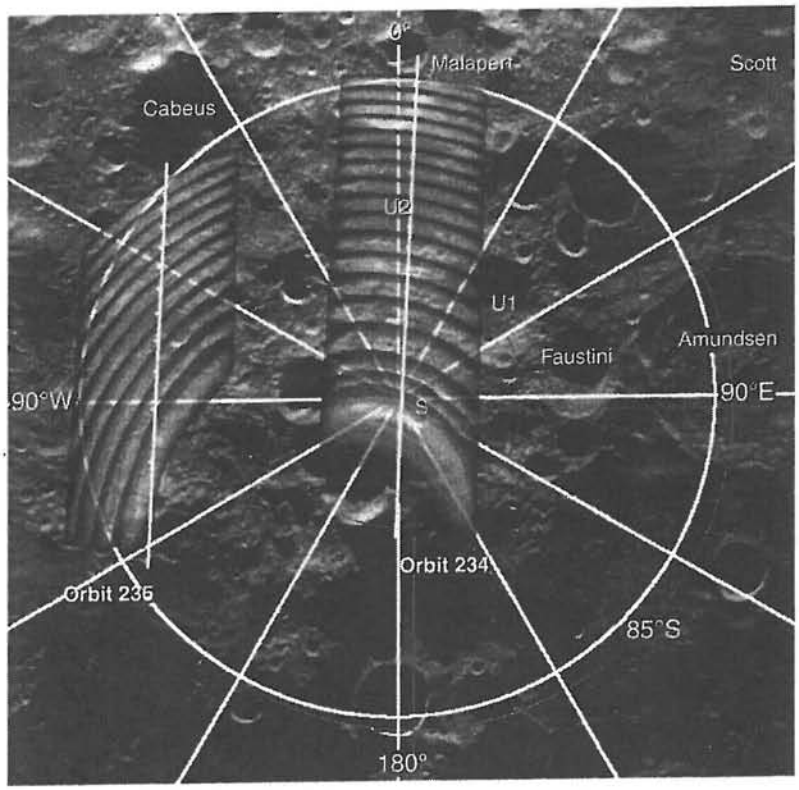
0°
Malapert
Scott
Cabeus
U2
U1
Amundsen
Faustini
90°W
90°E
S
Orbit 234
Orbit 235
85°S
180°

Fig. 1

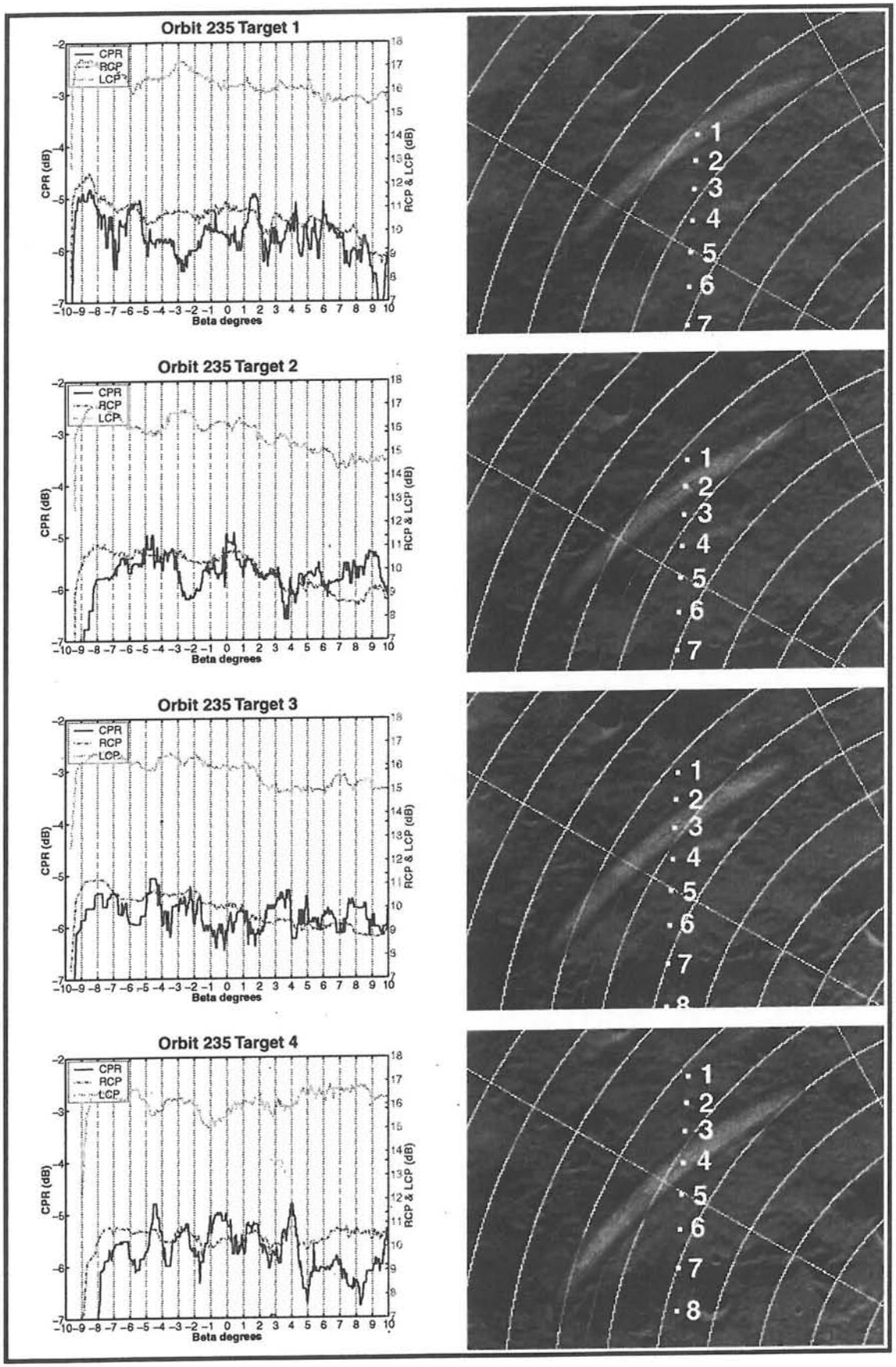
Orbit 235 Target 1
CPR
RCP
LCP
CPR (dB)
RCP & LCP (dB)
Beta degrees
1
2
3
4
5
6
7
Orbit 235 Target 2
CPR
RCP
LCP
CPR (dB)
RCP & LCP (dB)
Beta degrees
1
2
3
4
5
6
7
Orbit 235 Target 3
CPR
RCP
LCP
CPR (dB)
RCP & LCP (dB)
Beta degrees
1
2
3
4
5
6
7
Orbit 235 Target 4
CPR
RCP
LCP
CPR (dB)
RCP & LCP (dB)
Beta degrees
1
2
3
4
5
6
7
8

Fig. 2a

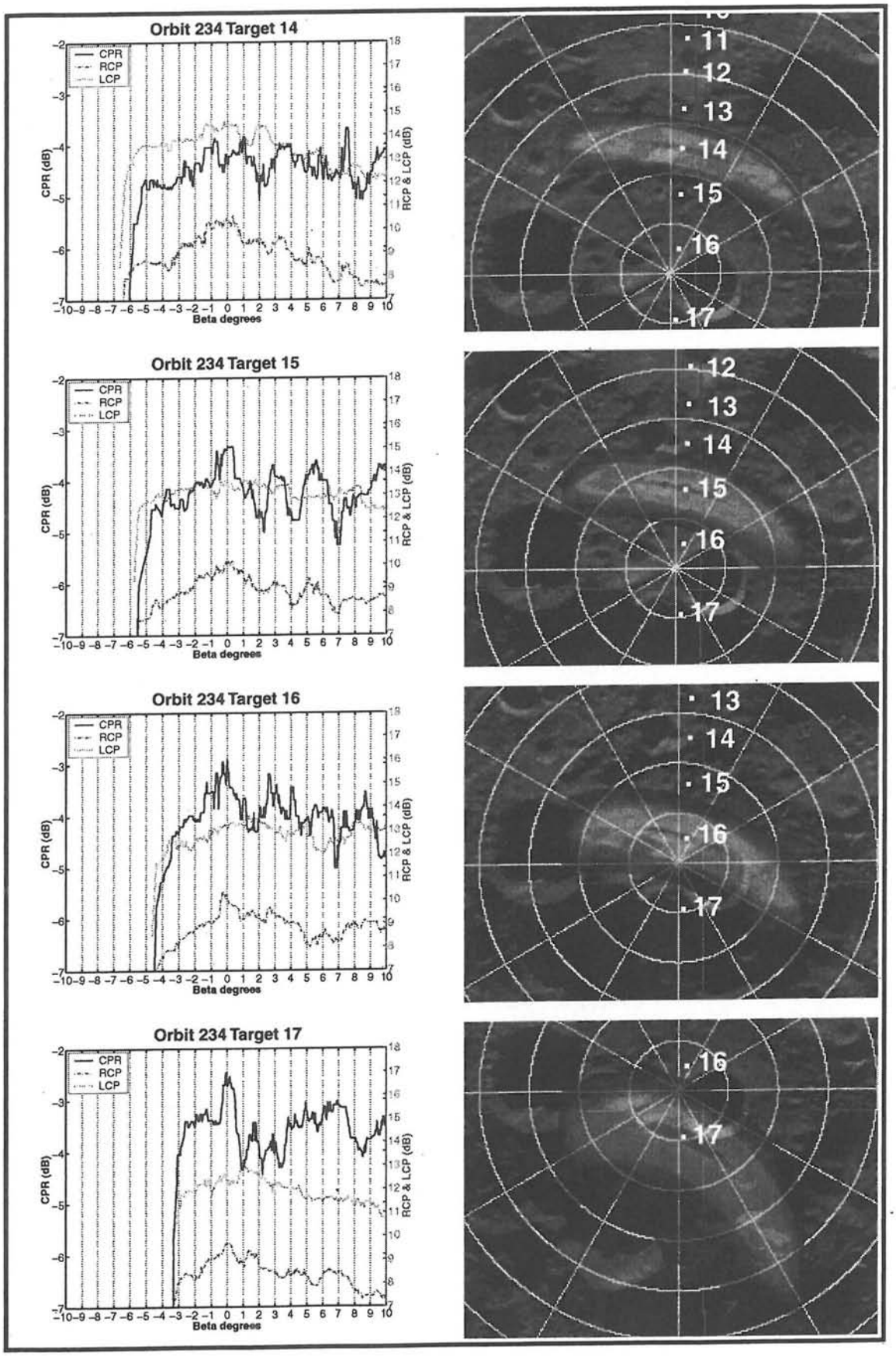
Orbit 234 Target 14
CPR
RCP
LCP
CPR (dB)
RCP & LCP (dB)
Beta degrees
11
12
13
14
15
16
17
Orbit 234 Target 15
CPR
RCP
LCP
CPR (dB)
RCP & LCP (dB)
Beta degrees
12
13
14
15
16
17
Orbit 234 Target 16
CPR
RCP
LCP
CPR (dB)
RCP & LCP (dB)
Beta degrees
13
14
15
16
17
Orbit 234 Target 17
CPR
RCP
LCP
CPR (dB)
RCP & LCP (dB)
Beta degrees
16
17

Fig. 2b

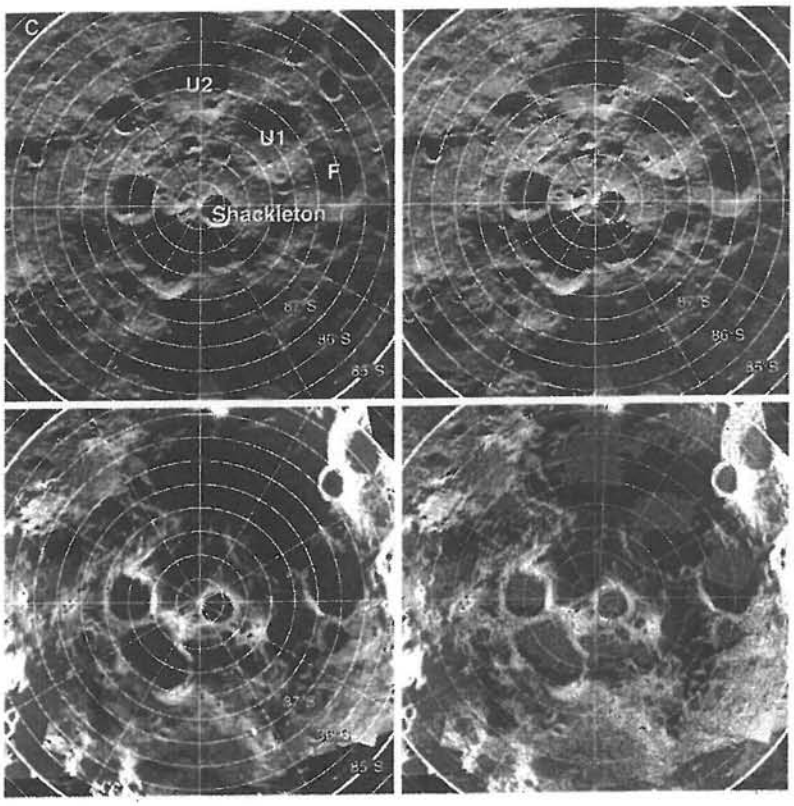

Fig. 3

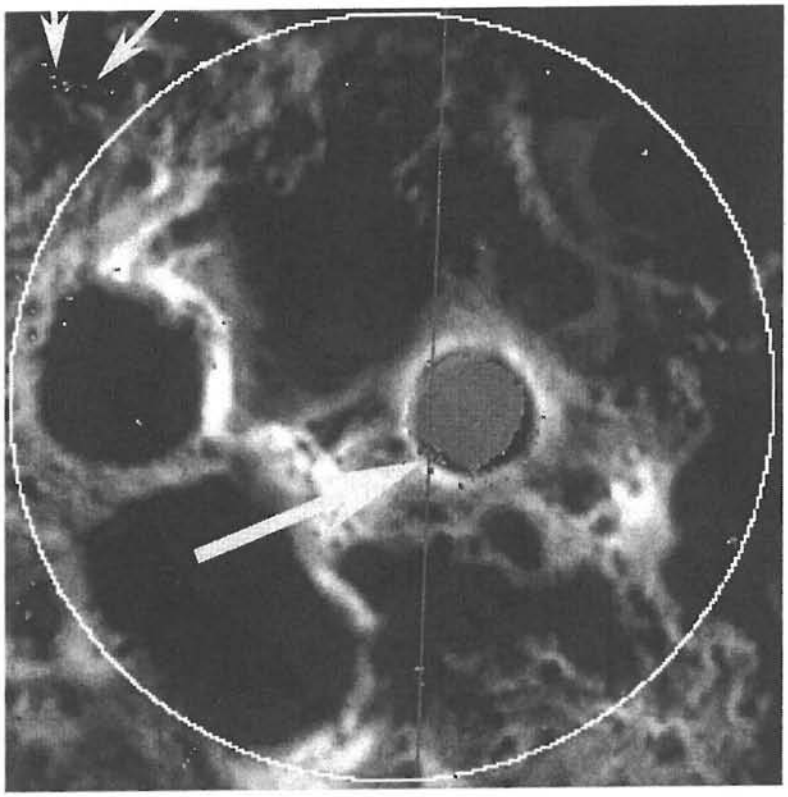

Fig. 4

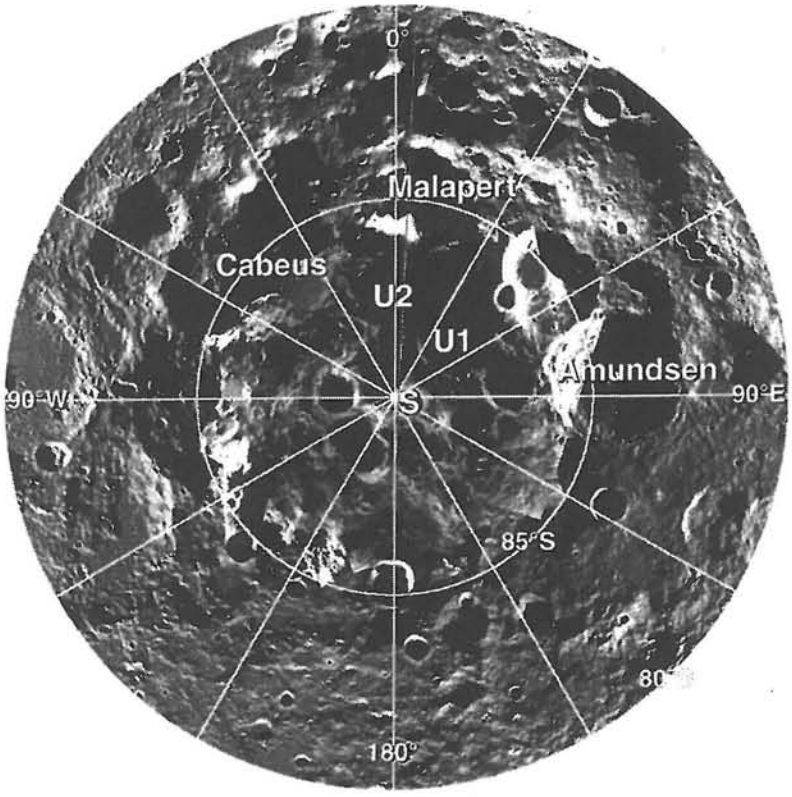
0°
Malapert
Cabeus
U2
U1
Amundsen
90°W
S
90°E
85°S
80°
180°

Fig. 5a

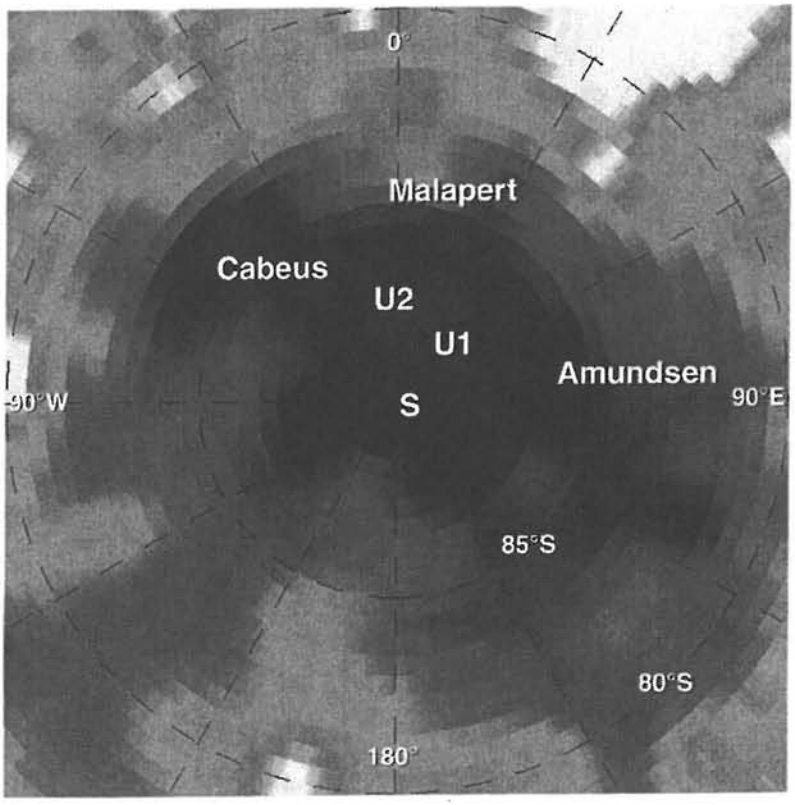
0°
Malapert
Cabeus
U2
U1
Amundsen
90°W
S
90°E
85°S
80°S
180°

Fig. 5b

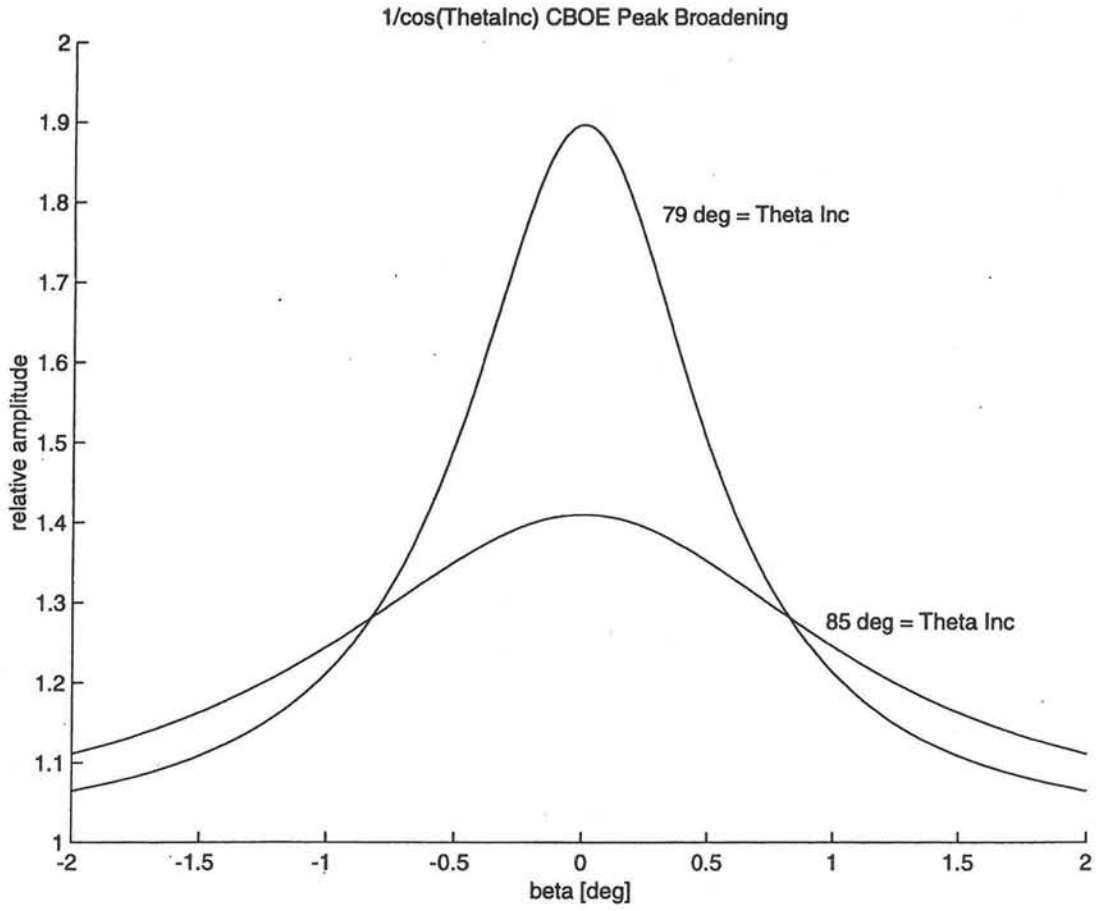
1/cos(ThetaInc) CBOE Peak Broadening
relative amplitude
beta [deg]
79 deg = Theta Inc
85 deg = Theta Inc
2
1.9
1.8
1.7
1.6
1.5
1.4
1.3
1.2
1.1
1
-2
-1.5
-1
-0.5
0
0.5
1
1.5
2

Fig. 6

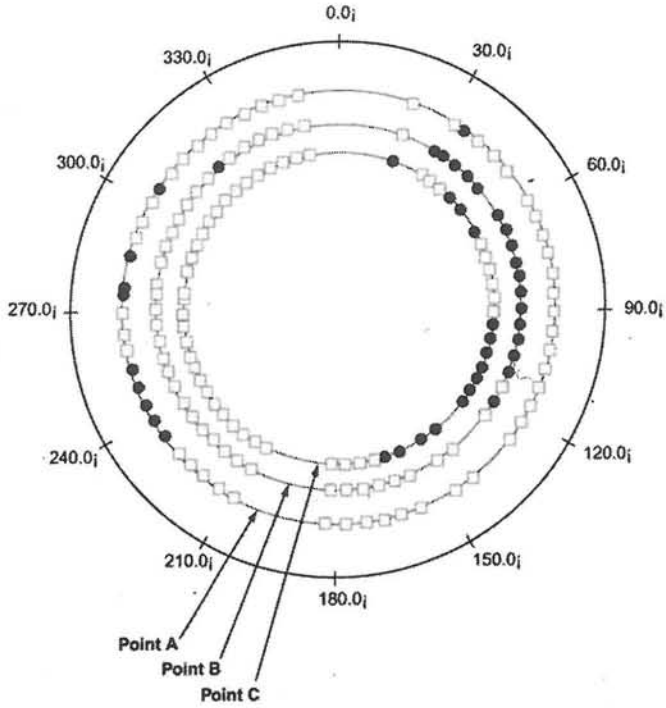
0.0¡
30.0¡
60.0¡
90.0¡
120.0¡
150.0¡
180.0¡
210.0¡
240.0¡
270.0¡
300.0¡
330.0¡
Point A
Point B
Point C

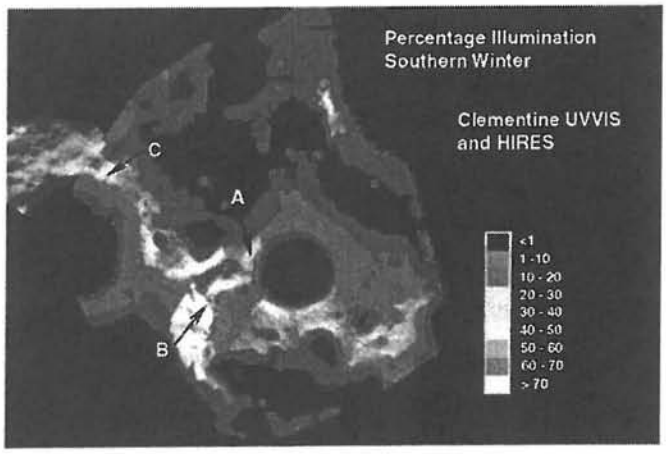
Percentage Illumination
Southern Winter
Clementine UVVIS
and HIRES
C
A
B
<1
1 - 10
10 - 20
20 - 30
30 - 40
40 - 50
50 - 60
60 - 70
> 70

Fig. 7